Complex-anisotropy-induced pattern formation in bistable media

Zhi Zhu He[1] and Jing Liu[1,2,*]

[1]*Key Laboratory of Cryogenics, Technical Institute of Physics and Chemistry, Chinese Academy of Sciences, Beijing 100190, China*

[2]*Department of Biomedical Engineering, School of Medicine, Tsinghua University, Beijing 100084, China*

(Received 16 April 2008; revised manuscript received 1 December 2008; published 6 February 2009)

A construct of anisotropy in bistable media is adopted to characterize the effects of anisotropy on pattern formation by means of anisotropic line tension. A velocity curvature relation is further derived to account for the anisotropic wave propagations. Stability analysis of transverse perturbations indicates that a sufficiently strong complex anisotropy can induce dynamical instabilities and even lead to a breakup of the wave patterns. Numerical simulations show that complex anisotropy can induce rich spatiotemporal behaviors in bistable media. The results of analysis and simulations demonstrate that this method successfully incorporates complex anisotropy into the reaction diffusion model and has general significance.

DOI: 10.1103/PhysRevE.79.026105 PACS number(s): 82.40.Ck, 82.40.Bj, 05.45.−a, 87.10.−e

I. INTRODUCTION

Nonequilibrium systems often exhibit various spatiotemporal patterns, which have been extensively investigated in many fields, such as physical, chemical, and biological systems [1]. Among the many phenomena ever observed before, the prominent experiments are generally focused on chemical waves such as those occurring at the catalytic surface [2], the rhythm in the cardiac tissue [3], and so on, in which the interplay between nonlinear reaction kinetics and diffusion of species can produce rich spatiotemporal patterns.

Many existing studies mainly concentrate on isotropic systems, where the speed of species diffusion is identical in all directions and independent of the system state. However, for a realistic medium, which is often anisotropic, the normal velocity of a chemical wave depends on its propagation direction. As is gradually realized, anisotropy may induce new dynamical state and distinctive patterns. Anisotropic reaction diffusion systems have attracted considerable attention in experimental and theoretical studies. Some novel phenomena unobservable in isotropic systems, such as reaction diffusion waves with sharp corners [4], traveling-wave fragments along a preferred orientation [5], and stratified spatiotemporal chaos characterized by strong correlations along a principal direction [6], were discovered in anisotropic media.

The anisotropy of a system is originally induced by the intrinsic inhomogeneity of the media, such as inhomogeneous substrate corrugation of a catalytic surface [7,8] or medium deformation due to external force such as distortion of cardiac tissue [9]. For a constant anisotropic diffusion coefficient tensor, propagation of the wave is dependent on its orientation and independent of the state of the system. For example, an Ising front would transform into a Bloch front when the propagation directions of a wave change from the x axis to the y axis in a two-dimensional bistable medium with constant anisotropic diffusion coefficient [10]. Such anisotropy may strongly influence the dynamical behavior of a nonstationary system, even induce new dynamical states [6]. In general, a constant anisotropic diffusion coefficient tensor can be easily removed by rescaling the spatial coordinates, while a complex anisotropy is often dependent on the system state, which cannot be eliminated by such a transformation. For a nontrivial system, the state-dependent diffusion can lead to dynamical state variation along the profile of a wave front [4]. However, it is rather difficult to use reaction diffusion equations to study pattern formation induced by complex anisotropy and identify its influence on the chemical wave propagation in bistable media. The main difficulty lies in the incorporation of complex anisotropy into the reaction diffusion model. This paper is dedicated to construct a general anisotropy expression for the reaction diffusion model and thus investigate pattern formation induced by complex anisotropy in bistable media.

The interface of high and low concentrations of species, called wave front in the bistable system, has an important influence on the dynamical state of the system. A nonlocal contour dynamics model for interface motion has been developed in two-dimensional isotropic bistable systems [11,12]. It was shown that the chemical front motion is determined by a nonlocal Lyapunov energy, which is partitioned into three contributions: an effective line tension, a pressure, and a nonlocal coupling force between fronts. It is noteworthy that the line tension is considered as constant in the isotropic system. However, for an anisotropic case, the wave front motion is strongly dependent on the orientation of the wave propagation, which may be due to the orientational dependence of the line tension. In this paper, the anisotropy is absorbed into the bistable system by constructing an anisotropic line tension, which is similar to that in crystal growth [13]. Such a method can effectively characterize the normal propagation velocity of a chemical wave dependent on the propagation direction in the anisotropic bistable media. Further, a velocity-curvature relation of the wave front is derived to study a nonequilibrium Ising-Bloch (NIB) bifurcation and transverse instability of planar fronts, and confirm the influence of complex anisotropy on pattern formation. In addition, numerical simulations demonstrate that complex anisotropy can induce some new patterns, such as polygon-shaped patterns (target structures and spiral waves) and di-

*Address for correspondence: P.O. Box 2711, Technical Institute of Physics and Chemistry, Chinese Academy of Sciences, Beijing 100190, China. FAX: +86-10-82543767. jliu@mail.ipc.ac.cn

rectional stripes, which possibly cannot be observed in isotropic or simple anisotropic bistable media.

II. GENERAL EXPRESSION FOR ANISOTROPY IN THE REACTION DIFFUSION MODEL

In this paper, the FitzHugh-Nagumo models [14], which can exhibit abundant features of bistable media with proper parameters, are adopted as follows:

$$\frac{\partial u}{\partial t} = \delta^{-1}\nabla^2 u + \varepsilon^{-1}(u - u^3 - v), \quad \frac{\partial v}{\partial t} = \nabla^2 v + (u - a_1 v - a_0), \tag{1}$$

where u represents the activator and v is the inhibitor. The parameter δ denotes the ratio between the diffusion coefficients of (u,v). The parameter $\varepsilon > 0$ characterizes the time scales associated with evolution of u and v. With proper choice of a_1 and a_0, Eqs. (1) can describe a bistable medium with two stationary and uniform stable states, an up state (u_+, v_+) and a down state (u_-, v_-), $(u_+, v_+) = -(u_-, v_-)$ for $a_0 = 0$, especially. For $\mu = \sqrt{\varepsilon/\delta} \ll 1$, the NIB bifurcation boundary is determined by $\delta = \eta_c^2/\varepsilon$ (or $\eta = \eta_c$) in the parameters space (ε, δ), where $\eta_c = 3/(2\sqrt{2}q^3)$, with $q^2 = a_1 + 1/2$ and $\eta = \sqrt{\varepsilon\delta}$. The single stationary front (an "Ising" front) will lose stability to a pair of counterpropagating fronts ("Bloch" front) when η changes from $\eta > \eta_c$ to $\eta \leqslant \eta_c$ [15]. Various pattern formations, such as spiral waves, labyrinths, breathing spots, and self-replication spots, have been observed in the bistable system [16].

It is noteworthy for $\varepsilon \ll 1$ that the v field remains approximately constant on the length scale over which u varies. In the narrow regions near the wave front defined by the contour of $u = 0$, where u varies steeply from u_+ to u_- along the normal to the wave front and v can be approximately considered as constant v_f, Eqs. (1) can be approximately expressed in a variational form

$$\frac{\partial u}{\partial t} = -\frac{\delta F}{\delta u}, \quad v = v_f, \tag{2}$$

where F is a Lyapunov function:

$$F = \int \left[\varepsilon^{-1} f(u, v_f) + \frac{1}{2}\delta^{-1}|\nabla u|^2 \right] d\mathbf{x},$$

$$f(u, v_f) = -\frac{u^2}{2} + \frac{u^4}{4} + u v_f. \tag{3}$$

Equations (2) indicate that the front solutions of Eqs. (1) propagate in a preferred direction dictated by the minimization of F. In other words, the velocity and orientation of the wave propagation are both determined by the partial distribution of F. In fact, Eqs. (2) can be described by the terminology of equilibrium phase transitions, where u is equal to an order parameter, v is the external field, and F represents the free energy.

We first consider a bistable medium composed of a circle-shaped island of $u_{in} \approx u_+$ embedded in an infinite sea of $u_{out} \approx u_-$. We note that the square gradient term in Eqs. (3) has only limited utility in domains near the interface of u_+/u_-. The nonlocal contour dynamics [11] shows that the integral of $\frac{1}{2}\delta^{-1}|\nabla u|^2$ is equal to $\oint \gamma(s) ds$, which can be reduced to $2\pi R \gamma_{iso}$ for the isotropic system, where R is the radius of the island and $\gamma_{iso} \approx \delta^{-1}(u_{in} - u_{out})^2 / 2l$ is interpreted as the line tension with l as the characteristic length scale of the profile. The line tension for the isotropic system, which can be found exactly from the one-dimensional asymptotics [12], is independent of the normal orientation of the interface. On the contrary, for the anisotropic case, the line tension of the u_+/u_- interface may vary along the profile of the interface. The square gradient term for a simple anisotropy should be written as $\frac{1}{2}\delta^{-1}[u_x^2 + (1+d)u_y^2]$, with constant anisotropy parameter $d > 0$. It can be rewritten as the form $\frac{1}{2}\delta^{-1}\gamma^2(\boldsymbol{\nu})|\nabla u|^2$, where $\boldsymbol{\nu} = \nabla u/|\nabla u|$ is the unit normal vector of the interface. $\gamma(\boldsymbol{\nu})$ may be considered as a dimensionless anisotropic line tension. It is easy to determine $\gamma(\boldsymbol{\nu}) = \sqrt{1 + d\sin^2\phi}$ for the simple anisotropy, where ϕ is the angle that the normal to the interface makes with the x axis and satisfies the relation $\boldsymbol{\nu} = \cos\phi \mathbf{x} + \sin\phi \mathbf{y}$ with $\mathbf{x}$ and $\mathbf{y}$ unit coordinate vectors in the Cartesian coordinate system. Thus the line tension varies along the profile of the island and reaches a minimum in the direction of the x axis and becomes maximum along the orientation of the y axis. The integral of the square gradient term is equal to $2\pi R \gamma_{iso}(1+d)$ for the simple anisotropy.

From the above dissection, $\frac{1}{2}\delta^{-1}(\nabla u)^2$ can be replaced by the form $\frac{1}{2}\delta^{-1}\gamma^2(\nabla u)$ without losing generality. Thus it is straightforward to derive the following expression by taking the variation of the Lyapunov function as

$$\frac{\partial u}{\partial t} = \delta^{-1}\left[\frac{\partial}{\partial x}\left(\gamma(\nabla u)\frac{\partial \gamma(\nabla u)}{\partial u_x} \right) + \frac{\partial}{\partial y}\left(\gamma(\nabla u)\frac{\partial \gamma(\nabla u)}{\partial u_y} \right) \right] + \varepsilon^{-1}(u - u^3 - v). \tag{4}$$

In this paper, γ is assumed to be a homogenous function $\gamma(\nabla u) = \gamma(\boldsymbol{\nu})|\nabla u|$, so that Eq. (4) can be modified as

$$\frac{\partial u}{\partial t} = \delta^{-1}\nabla \cdot [\gamma^2 \nabla u + \gamma\gamma'(-u_y \mathbf{x} + u_x \mathbf{y})] + \varepsilon^{-1}(u - u^3 - v), \tag{5}$$

where $\gamma = \gamma(\phi)$ and $\gamma' = \partial\gamma/\partial\phi$. Therefore, for anisotropic bistable media, Eqs. (1) can be rewritten as

$$\frac{\partial u}{\partial t} = \delta^{-1}\nabla \cdot (\mathbf{D}\nabla u) + \varepsilon^{-1}(u - u^3 - v),$$

$$\frac{\partial v}{\partial t} = \nabla^2 v + (u - a_1 v - a_0), \tag{6}$$

where $\mathbf{D}$ is considered as a dimensionless diffusion coefficient tensor and represents the anisotropy:

$$\mathbf{D} = \begin{pmatrix} \gamma^2 & -\gamma\gamma' \\ \gamma\gamma' & \gamma^2 \end{pmatrix}. \tag{7}$$

Equation (7) can be reduced to the isotropic case with $\gamma = 1$, the simple anisotropic case with $\gamma = \sqrt{1 + d\sin^2\phi}$, and the rotational anisotropic case with $\gamma = \sqrt{1 + d\sin^2(\phi - \Theta)}$, where

Θ represents the rotational angle, such as the fiber orientation in cardiac tissue [17]. For complex anisotropy, the expression of $\gamma(\boldsymbol{\nu})$ may be very complex and has no unified form. One alternative choice may be $\gamma=\sqrt{q_1(\phi)\cos^2\phi+q_2(\phi)\sin^2\phi}$ [4], where both $q_1(\phi)$ and $q_2(\phi)$ are a function of ϕ. Another choice is $\gamma=1+\alpha\cos(m\phi)$ [18], where α is the intensity of the anisotropy and m represents the symmetry of the system. Equation (7) indicates that the generalized anisotropy expression is embedded in the reaction diffusion model by constructing a dimensionless anisotropic line tension $\gamma(\boldsymbol{\nu})$, which depends on the normal orientation of the wave front. In fact, $\mathbf{D}_u$ may be significant only in the neighborhood of the wave front where $|\nabla u|$ is non-negligible, so that it can be expanded to the whole domain.

III. VELOCITY CURVATURE RELATION AND TRANSVERSE INSTABILITY OF PLANAR FRONTS

We study the effects of the anisotropy on the chemical waves in bistable media by deriving velocity curvature relations for nearly planar fronts with small curvature, which has been proven to be a useful tool for a qualitative description of complex dynamic processes [15]. A singular perturbation approach is adopted to obtain velocity-curvature relations, which is valid for the small parameter μ.

It is convenient to introduce a local moving orthogonal coordinate system

$$\mathbf{r}=\mathbf{R}(s,t)+r\mathbf{n}(s), \tag{8}$$

where $\mathbf{r}$ is the position vector of a point near the wave front, $\mathbf{R}$ represents the position of the wave front, $\mathbf{n}=\cos\theta\mathbf{x}+\sin\theta\mathbf{y}$ is the unit normal vector of the wave front with θ the angle that the normal to the wave front makes with the x axis, and s is the arclength along the wave front. It is easy to describe orthogonal coordinate basis vectors in

$$\mathbf{e}_r=\frac{\partial\mathbf{r}}{\partial r}=\mathbf{n}(s),\quad \mathbf{e}_s=\frac{\partial\mathbf{r}}{\partial s}=(1+r\kappa)\boldsymbol{\tau}, \tag{9}$$

where $\boldsymbol{\tau}=\partial\mathbf{R}/\partial s$ is the unit tangent vector to the wave front and the curvature is $\kappa=\partial\theta/\partial s$. The determinant of the metric tensor is therefore given by $g=\det(\mathbf{e}_\alpha\mathbf{e}_\beta)=(1+r\kappa)^2$, where $\alpha,\beta\in\{r,s\}$. Then, the gradient and divergence can be expressed as

$$\nabla u=u_r\mathbf{n}+\sqrt{g}^{-1}u_s\boldsymbol{\tau},\quad \nabla\cdot\mathbf{A}=\sqrt{g}^{-1}[(\sqrt{g}A_1)_r+(A_2)_s], \tag{10}$$

where $\mathbf{A}=A_1\mathbf{n}+A_2\boldsymbol{\tau}$. Furthermore, we get

$$-u_y\mathbf{x}+u_x\mathbf{y}=-\sqrt{g}^{-1}u_s\mathbf{n}+u_r\boldsymbol{\tau}. \tag{11}$$

For $\mu\ll1$, the narrow regions along the normal to the wave front, where $\partial u/\partial r\approx O(\mu^{-1})$ and $\partial v/\partial r\approx O(1)$, are considered as inner regions. In addition, both $\partial u/\partial r$ and $\partial v/\partial r$ are of order unity in the outer regions. The dynamics in the inner regions is studied by introducing a stretched normal coordinate $\rho=r/\mu$, with corresponding expansions

$$u(r,s,t)=u^{(0)}(\rho,s,t)+\mu u^{(1)}(\rho,s,t)+\mu^2u^{(2)}(\rho,s,t)+\cdots,$$

$$v(r,s,t)=v^{(0)}(\rho,s,t)+\mu v^{(1)}(\rho,s,t)+\mu^2v^{(2)}(\rho,s,t)+\cdots. \tag{12}$$

The time derivative now becomes

$$\frac{\partial u}{\partial t}=\frac{\partial u^{(0)}}{\partial t}-V_n\frac{\partial u^{(0)}}{\partial\rho}+\dot{s}\frac{\partial u^{(0)}}{\partial s}+O(\mu), \tag{13}$$

where $\dot{s}=\partial s/\partial t$ and $V_n=-\partial\rho/\partial t$ is the front velocity in a direction normal to the wave front. Expansion of $\boldsymbol{\nu}$ is found by

$$\begin{aligned}\boldsymbol{\nu}&=\frac{\nabla u}{|\nabla u|}=\frac{u_\rho\mathbf{n}+\mu(1+\mu\rho\kappa)^{-1}u_s\boldsymbol{\tau}}{[u_\rho^2+\mu^2(1+\mu\rho\kappa)^{-2}u_s^2]^{1/2}}\\&=-\left(\mathbf{n}+\mu\frac{u_s^{(0)}}{u_\rho^{(0)}}\boldsymbol{\tau}\right)+O(\mu^2),\end{aligned} \tag{14}$$

where we assume that $u_\rho^{(0)}<0$ [see Eq. (18)]. From Eq. (14), one can conclude

$$\gamma(\phi)=\tilde{\gamma}(\theta)+\mu\tilde{\gamma}'(\theta)u_s^{(0)}/u_\rho^{(0)}+O(\mu^2), \tag{15}$$

where $\tilde{\gamma}'(\theta)=\partial\tilde{\gamma}(\theta)/\partial\theta$. It is noted that $\partial\tilde{\gamma}(\theta)/\partial s=\kappa\tilde{\gamma}'(\theta)$. The expansion of diffusion term in Eq. (5) can be written as

$$\begin{aligned}&\nabla\cdot[\gamma^2\nabla u+\gamma\gamma'(-u_y\mathbf{x}+u_x\mathbf{y})]\\&=\sqrt{g}^{-1}\{[\sqrt{g}\gamma^2u_r-\gamma\gamma'u_s]_r+[\gamma\gamma'u_r+\sqrt{g}^{-1}\gamma^2u_s]_s\}\\&=\mu^{-2}\tilde{\gamma}^2u_{\rho\rho}^{(0)}+\mu^{-1}[\tilde{\gamma}^2u_{\rho\rho}^{(1)}+2\tilde{\gamma}\tilde{\gamma}'u_{\rho s}^{(0)}]\\&\quad+\mu^{-1}[(\tilde{\gamma}')^2+\tilde{\gamma}\tilde{\gamma}''+\tilde{\gamma}^2]\kappa u_\rho^{(0)}+O(1).\end{aligned} \tag{16}$$

The expansion of reaction term is given by

$$\begin{aligned}u-u^3-v&=[u^{(0)}-(u^{(0)})^3-v_f^{(0)}]+\mu[1-(u^{(0)})^2]u^{(1)}\\&\quad+\mu v_f^{(1)}+O(\mu^2).\end{aligned} \tag{17}$$

Substituting Eqs. (13), (16), and (17) into Eq. (5), the zeroth-order stationary wave front solution of Eq. (6) is found by

$$u^{(0)}=-\tanh\left(\frac{\rho}{\tilde{\gamma}\sqrt{2}}\right),\quad v_f^{(0)}=0. \tag{18}$$

The first-order solution is given by

$$\begin{aligned}Lu^{(1)}&=v_f^{(1)}+\eta(u_t^{(0)}-V_nu_\rho^{(0)}+\dot{s}u_s^{(0)})\\&\quad-\kappa[\tilde{\gamma}^2+(\tilde{\gamma}')^2+\tilde{\gamma}\tilde{\gamma}'']u_\rho^{(0)}+2\tilde{\gamma}\tilde{\gamma}'u_{\rho s}^{(0)},\end{aligned} \tag{19}$$

where $L=\partial^2\tilde{\gamma}/\partial\rho^2+[1-3(u^{(0)})^2]$. Since $Lu_\rho^{(0)}=0$, the right-hand side of Eq. (19) must be orthogonal to $u_\rho^{(0)}$, which is called the solvability followed by

$$\begin{aligned}&\eta V_n\int_{-\infty}^{+\infty}\left(\frac{\partial u^{(0)}}{\partial\rho}\right)^2d\rho\\&=\int_{-\infty}^{+\infty}v_f^1\frac{\partial u^{(0)}}{\partial\rho}d\rho+\int_{-\infty}^{+\infty}\eta\left(\frac{\partial u^{(0)}}{\partial\tau}+\dot{s}\frac{\partial u^{(0)}}{\partial s}\right)\frac{\partial u^{(0)}}{\partial\rho}d\rho\\&\quad-\kappa[\tilde{\gamma}^2+(\tilde{\gamma}')^2+\tilde{\gamma}\tilde{\gamma}'']\int_{-\infty}^{+\infty}\left(\frac{\partial u^{(0)}}{\partial\rho}\right)^2d\rho\\&\quad+\tilde{\gamma}\tilde{\gamma}'\frac{d}{ds}\left[\int_{-\infty}^{+\infty}\left(\frac{\partial u^{(0)}}{\partial\rho}\right)^2d\rho\right].\end{aligned} \tag{20}$$

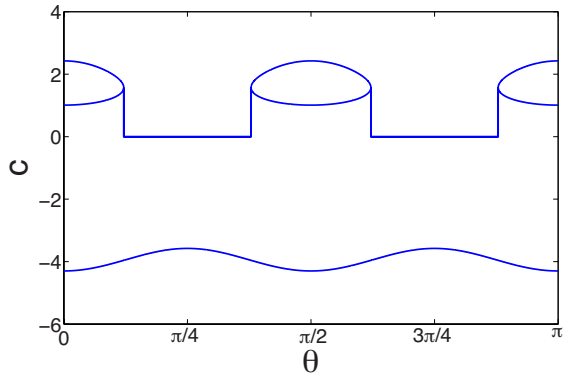

FIG. 1. (Color online) Under the choice $\gamma=1+0.04\cos(4\theta)$, the velocity of planar ($\kappa=0$) fronts at different angles. The Ising fronts exist in all directions, while the Bloch fronts exist in narrow regimes around $\theta=0$, $\theta=\pi/2$, and $\theta=\pi$.

According to Eq. (18), Eq. (20) can be reduced to

$$C_n=-\frac{3\tilde{\gamma}}{\sqrt{2}\eta}v_f-\delta^{-1}\tilde{\gamma}(\tilde{\gamma}+\tilde{\gamma}')\kappa, \tag{21}$$

where $V_n=\mu C_n$ and $v_f^{(1)}=\mu v_f+O(\mu^2)$. For outer regions, the relation between v_f and C_n also can be found by (see Ref. [15])

$$v_f=-\frac{C_n+\kappa}{q^2\sqrt{(C_n+\kappa)^2+4q^2}}-\frac{a_0}{q^2}. \tag{22}$$

An implicit relation between the normal velocity of the front and its curvature is therefore deduced from Eqs. (21) and (22) by

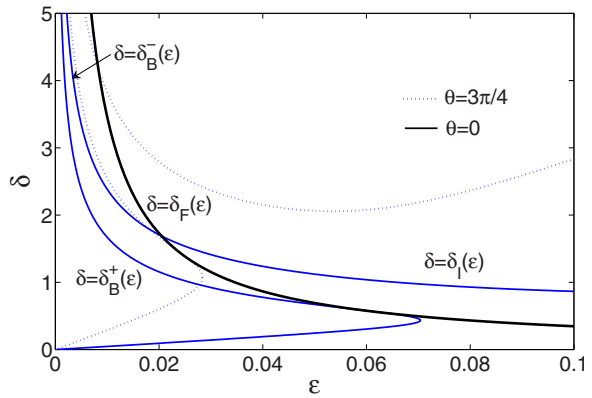

FIG. 2. (Color online) NIB bifurcation and planar front transverse instability boundaries in the (ε,δ) plane for the anisotropic $(\tilde{\gamma}=1+0.03\cos 4\theta)$ and nonsymmetric $(a_0=-0.1)$ systems. The thick curve denotes the front bifurcation. The thin lines present the transverse instability boundaries of Ising fronts with δ_I and Bloch fronts with δ_B. The dashed lines present wave propagation along the $\theta=3\pi/4$ direction; the dashed lines present wave propagation along the $\theta=0$ direction. The parameter $a_1=2.0$.

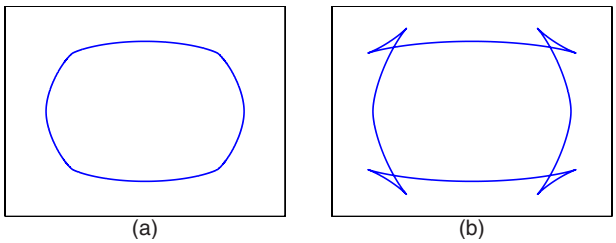

FIG. 3. (Color online) The "square-shaped" contour of stationary patterns ($C_n=0$) with complex anisotropy $\tilde{\gamma}=\sqrt{q_1(\theta)\cos^2\theta+q_2(\theta)\sin^2\theta}$ with $q_1(\theta)=2$ and $q_2(\theta)=1+b\sin^2 2\theta$. (a) The smooth contour for $b=0.5$ and (b) the contour with the outer loops ("swallow tails") for $b=1.5$. Such loops should be cut off because of no physical meaning.

$$C_n+\delta^{-1}\tilde{\gamma}(\tilde{\gamma}+\tilde{\gamma}')\kappa=\frac{3\tilde{\gamma}}{\eta\sqrt{2}}\left[\frac{C_n+\kappa}{q^2\sqrt{(C_n+\kappa)^2+4q^2}}+\frac{a_0}{q^2}\right]. \tag{23}$$

For the simple anisotropy $\tilde{\gamma}=\sqrt{1+d\sin^2\theta}$, Eq. (23) can be reduced to

$$C_n+\delta^{-1}\frac{1+d}{\tilde{\gamma}^2}\kappa=\frac{3\tilde{\gamma}}{\eta\sqrt{2}}\left[\frac{C_n+\kappa}{q^2\sqrt{(C_n+\kappa)^2+4q^2}}+\frac{a_0}{q^2}\right], \tag{24}$$

which has been obtained in Ref. [15].

In the symmetric system ($a_0=0$), the planar front ($\kappa=0$) solutions are obtained from Eq. (23) with the Ising front solution as $C_0=0$ and the two Bloch front solutions as $C_0=\pm 2q\eta^{-1}\sqrt{\tilde{\gamma}^2\eta_c^2-\eta^2}$ for $\eta\leqslant\tilde{\gamma}\eta_c$, respectively. The threshold of the NIB bifurcation is found by $\eta_c^{ani}=\eta_c\tilde{\gamma}(1-a_0^{2/3})^{3/2}$. Under the choice of $\tilde{\gamma}=1+0.04\cos(4\theta)$, Fig. 1 gives the velocity of planar ($\kappa=0$) fronts at different angles according to Eq. (23). From Fig. 1, one can note that the existence of front solutions depends on the orientations of the wave propagation. For $\theta\in[0,\pi]$, the Ising fronts exist in all directions, while the Bloch fronts occur in narrow regimes around $\theta=0$, $\theta=\pi/2$, and $\theta=\pi$.

In order to study the stability of the Ising and Bloch fronts to transverse perturbations in the anisotropic bistable system,

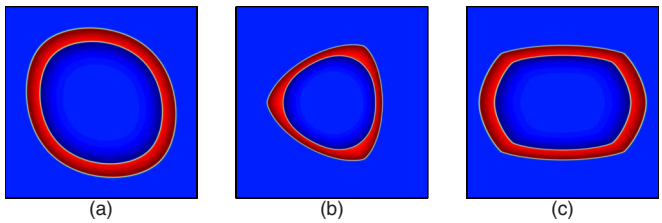

FIG. 4. (Color online) Polygon-shaped target waves induced by complex anisotropy with parameters corresponding to the stable Bloch fronts. (a) The elliptic target wave under the choice of $\gamma=\sqrt{q_1(\phi_1)\cos^2\phi_1+q_2(\phi_1)\sin^2\phi_1}$, with $q_1(\phi_1)=2$, $q_2(\phi_1)=1+0.5\sin^2\phi_1$, and $\phi_1=\phi+\pi/4$. (b) The triangular target wave with $\gamma=1+0.1\cos(3\phi)$. (c) The rectangular target wave with the same anisotropy form to (a) and $q_1(\phi_1)=2$, $q_2(\phi_1)=1+0.5\sin^2 2\phi_1$, and $\phi_1=\phi$. Parameters: $\delta=1.0$, $\varepsilon=0.02$

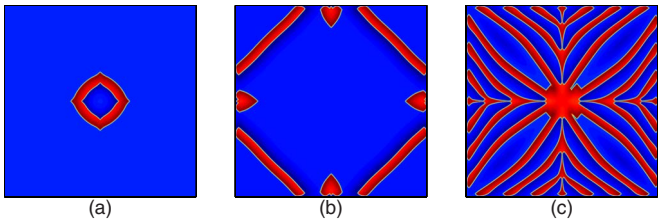

FIG. 5. (Color online) The breakup of a target wave is due to collision with the boundary of the system for complex anisotropy $\gamma=1+0.07\cos(4\phi)$. The initial condition is the same as that in Fig. 3. (a) $t=1$, (b) $t=8$, and (c) $t=20$. Parameters: $\delta=1.0$, $\varepsilon=0.02$.

we seek a relation of the form $C_n=C_0-D\kappa+O(\kappa^2)$ (around $\kappa=0$). If $D<0$, transverse instability occurs in the front solution, and its threshold of the planar front solution in parameters space (ε,δ) is obtained by setting $D=0$:

$$\delta_T=(\tilde{\gamma}+\tilde{\gamma}')\left(1+\frac{C_0^2}{4q^2}\right)^{3/2}\eta_c^{-1}\eta, \tag{25}$$

where it was supposed that $\tilde{\gamma}+\tilde{\gamma}'\geqslant 0$ satisfies all directions of the wave propagation. In the symmetric system $(a_0=0)$, the transverse instability threshold of the planar front solution is easily obtained by inserting the expression of C_0 into Eq. (25):

$$\delta_I=(\tilde{\gamma}+\tilde{\gamma}')^2\eta_c^{-2}\varepsilon, \quad \delta_B=\frac{\tilde{\gamma}\sqrt{\tilde{\gamma}(\tilde{\gamma}+\tilde{\gamma}')}\eta_c}{\sqrt{\varepsilon}}, \tag{26}$$

where the subscript I denotes the Ising fronts and B represents the Bloch fronts, while for the nonsymmetric case $(a_0\neq 0)$, the transverse instability threshold of the planar front solution cannot be obtained in such an explicit expression. Numerical solutions of Eq. (25) for the anisotropic $(\tilde{\gamma}=1+0.03\cos 4\theta)$ and nonsymmetric $(a_0=-0.1)$ systems are shown in Fig. 2, which predicts the front bifurcation and the transverse instability boundaries in different angles.

A sufficiently strong anisotropy makes the minimum of $\tilde{\gamma}+\tilde{\gamma}'$ negative (corresponding to $D<0$) along some orientations of the wave propagation. Therefore the chemical wave propagation will fail. For the simple anisotropy, $\tilde{\gamma}+\tilde{\gamma}'=(1+d)\tilde{\gamma}^{-3}$ is always positive and no such instability occurs.

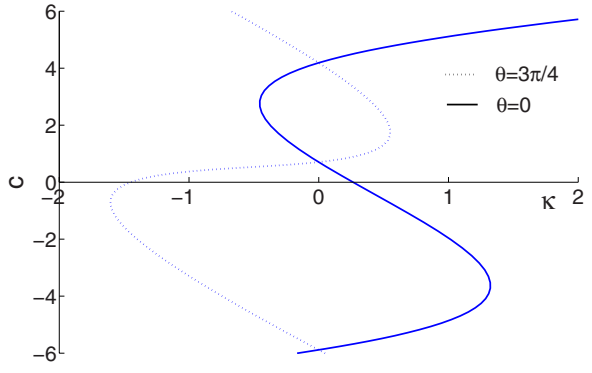

FIG. 6. (Color online) The velocity-curvature relation for different orientations of wave propagation. Parameters: $a_0=-0.1$, $a_1=2.0$, $\alpha=0.09$, $m=4$, $\delta=1.0$, $\varepsilon=0.02$.

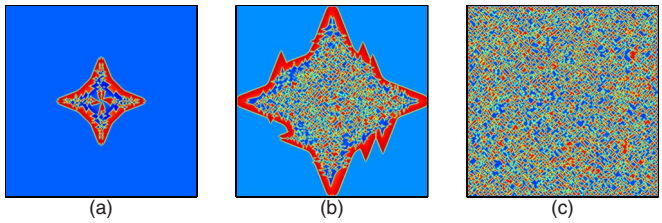

FIG. 7. (Color online) The breakup of a target wave is induced by the strong anisotropy $\gamma=1+0.09\cos(4\phi)$ and develops into spatiotemporal chaos finally. (a) $t=1$, (b) $t=3$, and (c) $t=170$. Parameters: $\delta=1.0$, $\varepsilon=0.02$.

Under the choice of complex anisotropy $\tilde{\gamma}=1+\alpha\cos(m\theta)$, the occurrence of $\tilde{\gamma}+\tilde{\gamma}'<0$ in some directions of wave propagation is equivalent to $\alpha>\alpha_c=(m^2-1)^{-1}$. According to Eq. (21), what was shown in Fig. 3 represents the square-shaped contour of a stationary pattern $(C_n=0)$ with complex anisotropy $\tilde{\gamma}=\sqrt{q_1(\theta)\cos^2\theta+q_2(\theta)\sin^2\theta}$. Figure 3(b) indicates that sufficiently strong anisotropy can lead to the occurrence of outer loops ("swallow tails"). Such swallow tails are not physically meaningful and should be replaced. A qualitative analysis of similar dynamics in excitable media has been discussed in Ref. [4]. From the above dissection, the complex anisotropy has been successfully expressed in the reaction diffusion model and can effectively describe chemical wave traveling in anisotropic bistable media.

IV. PATTERN FORMATION INDUCED BY COMPLEX ANISOTROPY

In this section we discuss pattern formation induced by complex anisotropy in the nonsymmetric $(a_0\neq 0)$ bistable system via numerical simulation. An explicit time-differencing scheme is adopted to solve Eqs. (6). All the simulations are performed in a two-dimensional 800×800 point grid $(\Delta x=10^{-1}$ and $\Delta t=10^{-3})$ with Neumann boundary conditions. The parameters $a_0=-0.1$ and $a_1=2.0$ are fixed for all simulations.

In the Bloch regimes of the bistable system, the traveling waves including target and spiral waves can be observed with proper initial conditions. Figure 4 shows how complex anisotropy induces the formation of polygon-shaped target waves. Figure 4(a) represents an elliptic target wave and indicates how the rotational angle Θ affects the wave propagation. Triangular waves have been observed in reactions on

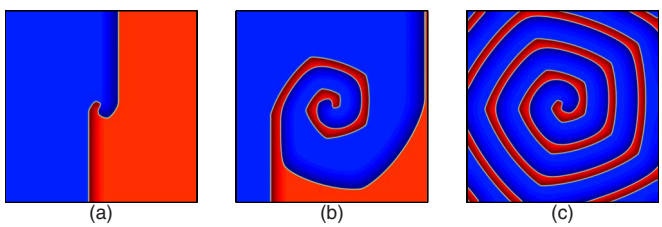

FIG. 8. (Color online) The development of a pentagon-shaped spiral wave with $\gamma=1+0.035\cos(5\phi)$ and parameters corresponding to the stable Bloch fronts. (a) $t=1$, (b) $t=6$, and (c) $t=50$. Parameters: $\delta=1.0$, $\varepsilon=0.025$.

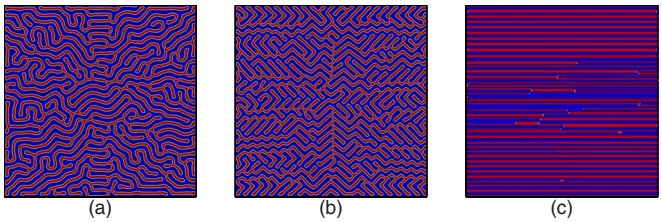

FIG. 9. (Color online) Pattern formation from a single stripe with transverse perturbation in its middle part [see Fig. 10(a)] in the unstable Ising regimes. (a) Labyrinthine pattern in the isotropic case, (b) comb-shaped stripes with $\gamma=1+0.04\cos(4\phi)$, and (c) directional stripes with $\gamma=\sqrt{2\cos^2\phi+q_2(\phi)\sin^2\phi}$ and $q_2(\phi)=1+0.5\sin^2\phi$. Parameters: $\delta=4.0$, $\varepsilon=0.045$.

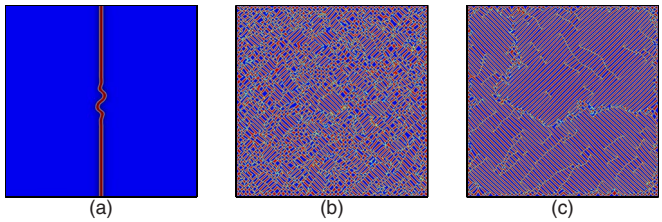

FIG. 10. (Color online) Under the choice of $\gamma=1+0.1\cos(4\phi)$, the development of directional stripes from a single stripe with transverse perturbation in its middle part. (a) $t=1$, (b) $t=50$, and (c) $t=420$. Parameters: $\delta=4.0$, $\varepsilon=0.045$.

the anisotropic catalytic surface [18]. Under the choice of complex anisotropy $\gamma=1+0.1\cos(3\phi)$, Fig. 4(b) shows a triangular target wave, where the parameter α may represent the magnitude of temperature or pressure, and m corresponds to the symmetrical surface structure according to Ref. [18]. The velocity of a single wave front has four maxima at different angles under the choice of $\gamma=\sqrt{2\cos^2\phi+q_2(\phi)\sin^2\phi}$, with $q_2(\phi)=1+0.5\sin^2 2\phi$. Thus a rectangular target wave [see Fig. 4(c)] can be observed under such a choice, which is very consistent with the qualitative dynamical analysis in Sec. III. Experiments have also observed hexagonal, diamond, and pentagonal geometries in chemical waves [8], which are attributed to the cellular inhomogeneities. Using the present model, one can easily reproduce these patterns by constructing a corresponding form of the anisotropy.

Numerical solutions show that polygon-shaped target waves under the choice of $\gamma=1+\alpha\cos(m\phi)$, with $\alpha<\alpha_c$, evolve from the circular wave and move stably away from the boundary of the media finally. If α increases to above α_c, such wave propagation is unstable and would disintegrate into segments due to colliding with the boundary of the system (see Fig. 5). The relation of C_n vs κ is shown in Fig. 6 for $\gamma=1+0.09\cos(4\theta)$. Both directions ($\theta=0$) and ($\theta=3\pi/4$) support pairs of counterpropagating Bloch fronts. But the positive slopes of cure of C_n vs κ in the direction ($\theta=0$) imply that wave propagations in such a direction are unstable to transverse perturbations. Figure 7 shows that the wave propagation runs to failure and develops into spatiotemporal chaos finally. Stratified spatiotemporal chaos with strong correlations along the principal direction has been observed in Ref. [6], where the dependence of front motion on the angle can illustrate the mechanism leading to stratified chaos. However, the segment chaos here is induced by strong anisotropy.

Figure 8 shows the development of a pentagon-shaped spiral wave evolving from an initial vortex structure due to the variation of propagation speeds at different directions. The rectangular spiral has been observed in the experiments [19]. It is easy to obtain the other polygon-shaped spiral waves in the stable bistable system with the proper choice of anisotropy form. Such polygon shaped patterns cannot appear in the simple anisotropy.

In the unstable Ising regimes, a stationary labyrinthine pattern in isotropic bistable media can be observed in Fig. 9(a) due to transverse instability. One important characteristic of such a pattern is that the upstate domain is connected. Under the choice of $\gamma=1+0.04\cos(4\phi)$, Fig. 9(b) indicates stationary comb-shaped stripes, which are made up of directional fold stripes. The transverse perturbations prevail in some preferred directions (such as the x axis) and can be suppressed in others due to complex anisotropy and front interaction. A more distinctive example is shown in Fig. 9(c), that stripes are parallel oriented to the x axis with the choice of $\gamma=\sqrt{2\cos^2\phi+q_2(\phi)\sin^2\phi}$ and $q_2(\phi)=1+0.5\sin^2\phi$. As shown in Fig. 10, a single stripe develops into directional stripes for $\gamma=1+0.1\cos(4\phi)$. A single stripe at first evolves into disordered patterns composed of many small segments. Subsequently, the segments oriented in preferred directions grow at their tips and emerge into larger stripe-shaped segments so that directional stripes will form finally.

V. CONCLUSION

In summary, complex anisotropy has been successfully constructed to the reaction diffusion model by means of anisotropic line tension, which depends on the normal direction of the wave propagation. This method may have general signification and effectively characterize the effects of anisotropy on pattern formation. Such a method can be used to predict new chemical wave pattern formation and study related dynamical mechanisms. Numerical simulation indicated that complex anisotropy can induce various special spatiotemporal patterns. The breakup of waves has been observed due to sufficiently strong anisotropy. Finally, it should be noted that the method can be extended to study complex anisotropic excitable media [20]. Particularly, some theoretical issues such as complex rotational anisotropy in cardiac tissue could also be tackled in this way.

ACKNOWLEDGMENTS

This work was partially supported by the National Natural Science Foundation of China under Grant No. 50776097 and Tsinghua-Yue-Yuen Medical Sciences Fund.

[1] M. C. Cross and P. C. Hohenberg, Rev. Mod. Phys. **65**, 851 (1993).
[2] R. Imbihl and G. Ertl, Chem. Rev. (Washington, D.C.) **95**, 697 (1995).
[3] A. V. Panfilov, Chaos **8**, 57 (1998).
[4] A. Mikhailov, Phys. Rev. E **49**, 5875 (1994).
[5] F. Mertens, N. Gottschalk, M. Bar, M. Eiswirth, A. Mikhailov, and R. Imbihl, Phys. Rev. E **51**, R5193 (1995).
[6] M. Bar, A. Hagberg, E. Meron, and U. Thiele, Phys. Rev. Lett. **83**, 2664 (1999).
[7] A. Makeev, M. Hinz, and R. Imbihl, J. Chem. Phys. **114**, 9083 (2001).
[8] O. Steinbock, P. Kettunen, and K. Showalter, Science **269**, 1857 (1995).
[9] A. V. Panfilov, R. H. Keldermann, and M. P. Nash, Phys. Rev. Lett. **95**, 258104 (2005).
[10] A. Hagberg and E. Meron, Phys. Rev. Lett. **91**, 224503 (2003).
[11] D. M. Petrich and R. E. Goldstein, Phys. Rev. Lett. **72**, 1120 (1994).
[12] R. E. Goldstein, D. J. Muraki, and D. M. Petrich, Phys. Rev. E **53**, 3933 (1996).
[13] G. B. McFadden, A. A. Wheeler, R. J. Braun, S. R. Coriell, and R. F. Sekerka, Phys. Rev. E **48**, 2016 (1993).
[14] A. Hagberg and E. Meron, Nonlinearity **7**, 805 (1994).
[15] M. Bar, A. Hagberg, E. Meron, and U. Thiele, Phys. Rev. E **62**, 366 (2000).
[16] A. Hagberg and E. Meron, Phys. Rev. Lett. **72**, 2494 (1994).
[17] F. Fenton and A. Karma, Chaos **8**, 20 (1998).
[18] M. Monine, L. Pismen, M. Bar *et al.*, J. Chem. Phys. **117**, 4473 (2002).
[19] N. Gottschalk, F. Mertens, M. Bar, M. Eiswirth, and R. Imbihl, Phys. Rev. Lett. **73**, 3483 (1994).
[20] Z. Z. He and J. Liu, Europhys. Lett. **85**, 18003 (2009).